Widely-Tunable High-Power Semiconductor Disk Laser with Non-Resonant AR-Assisted Gain Element on Diamond Heat Spreader

C. Borgentun,[1] ***Student Member, IEEE*****, C. Hessenius,**[2] **J. Bengtsson,**[1]
M. Fallahi,[2] ***Member, IEEE*****, A. Larsson,**[1] ***Senior Member, IEEE***

[1] *Department of Microtechnology and Nanoscience (MC2), Chalmers University of Technology, 41296 Göteborg, Sweden*
[2] *College of Optical Sciences, University of Arizona, Tucson, Arizona 85721, USA*

DOI: 10.1109/JPHOT.2011.XXXXXXX

Manuscript received August 26, 2011; revised xx, 2011. First published xx, 2011. Current version published xx, 2011.

Abstract: We report on an optically pumped semiconductor disk laser with a wide wavelength tuning range and a high peak output power. This was achieved using a combination of efficient thermal management and a broadband gain element with carefully engineered spectral gain characteristics. For heat removal, a flip-chip bonding scheme on diamond was used. To provide high active mirror reflectance over a large wavelength region, the layered structure of the gain element formed a non-resonant sub-cavity assisted by an anti-reflective structure. A peak output power of more than 7.5 W and a tuning range of 32 nm around the center wavelength of 995 nm were obtained.

Index Terms: Tunable lasers, Semiconductor lasers, Multilayer interference coatings.

1. Introduction

Tunable semiconductor lasers are of interest in applications such as atomic physics, spectroscopy, and optical communication [1]–[4]. One particular research effort is the development of a semiconductor laser that combines wide wavelength tunability with high output power. A promising candidate, that is also able to provide high beam quality, is the optically pumped semiconductor disk laser (OP-SDL), or the vertical-external-cavity surface-emitting laser (VECSEL) as it is also referred to [5]–[7]. Recent research has focused on extending the tuning range of OP-SDLs while maintaining high output power and high beam quality. Notable are the results from Fan *et al.* extending the tuning range to 33 nm centered at 975 nm with 8 W peak power, though with the added complexity of a multi-chip cavity configuration [8], and Paajaste *et al.* achieving a full tuning range of 150 nm at a center wavelength of 2 μm, though with a peak power below 400 mW [9]. One approach to achieve high output power over a wide tuning range, introduced by Borgentun *et al.* [10], is to carefully engineer the gain element (GE) such that it provides a reflectance exceeding unity over a wide range of wavelengths already at moderate pump powers. In this report, we present results from experiments demonstrating the success of this one-chip approach when combined with an efficient heat removal scheme.

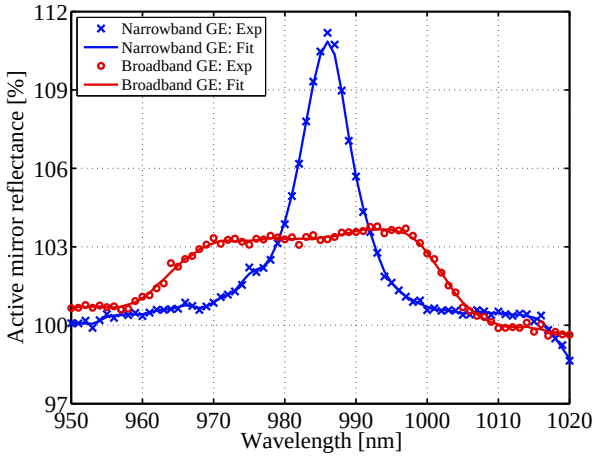

Fig. 1. Results from measurements of the AMR of two GEs: one conventional narrowband GE and one GE designed for a broad flat-top AMR spectrum. Exp: Experimental data, Fit: Smooth curve fit. Both GEs were optically pumped with the same incident pump power, i.e. 16.7 W focused to a spot of $\sim$500 μm diameter. The potential of the broadband GE for wide tunability is evident.

2. Gain Element Design

The GE of an OP-SDL can be seen as an active mirror with gain, i.e. the active mirror reflectance (AMR) exceeds 100% when pumped with sufficiently high pump power. Using numerical optimization, a GE was designed for a preferred dependence of the AMR on wavelength under certain pump conditions that would be beneficial for wide tunability. Specifically, the target AMR spectrum was set to be wide (40 nm centered at 980 nm) and flat-topped to reduce power variations over the tuning range. Details of the design can be found elsewhere [10] but we will here summarize the main design features that enable the AMR spectrum to come close to its target.

The broadband GE contains 12 InGaAs quantum wells (QWs) in six groups, separated by high-bandgap diffusion barriers to homogenize the populations of the QWs. The sub-cavity, formed by the layered structure containing the QWs, is anti-resonant at the center wavelength. Thus, as the wavelength deviates from the center wavelength the sub-cavity becomes increasingly resonant, thereby compensating the reduced material gain and the misalignment of the standing wave maxima with the QWs by an enhanced intra-sub-cavity field. Further, an epitaxial anti-reflection (AR) structure was added and parametrically optimized to fine-tune the AMR spectrum to its desired shape. The AR structure primarily moderates the strength of the sub-cavity resonance effect and consists of a stack of 2.5 $\sim \lambda/4$-thick pairs of alternating low- and high-index materials and a single $\sim \lambda/2$-thick layer of the high-index material.

The broadband properties of the optimized GE were quantitatively verified by comparing direct measurements of the AMR spectrum for the broadband GE with that of a conventional narrowband GE, see Fig. 1. The AMR spectra were measured by probing the reflectance of the optically pumped GEs using a tunable Ti:sapphire laser. The details of the measurement technique are presented elsewhere [11]. Even though the broadband tuning properties were evident also when the GE was used in an OP-SDL cavity and was pumped far above threshold [10], suboptimal heat removal was assumed to severely limit the performance. Therefore, in order to take full advantage of the sophisticated design of the GE and explore the limits of power and tunability, a more efficient thermal management scheme was needed.

3. Heat Removal

For efficient heat dissipation, the GEs were grown (by MOCVD) in reverse order, i.e. with the semiconductor distributed Bragg reflector (DBR) on top. A thin Ti/Au metallization layer was deposited on the epitaxial side of the cleaved wafer sample and on a chemical vapor deposited (CVD) diamond heat spreader, after which the sample was bonded to the heat spreader using indium solder. The main function of the heat spreader is to expand the basically one-dimensional heat flow inside the GE to three dimensions, which increases the dissipation capability of the heat sink. The GaAs substrate was then completely removed by a selective wet chemical etch, described in detail by Häring *et al.* [12], leaving only the DBR, the non-periodic gain region, and the optimized AR structure. Finally, the fully processed sample was mechanically mounted on a liquid-cooled copper heat sink for temperature control.

The thermal impedance of the heat removal scheme with the diamond heat spreader on a copper heat sink (henceforth referred to as the "diamond scheme") was evaluated and compared to the heat removal scheme used previously [10] with a copper heat spreader on a copper heat sink (henceforth referred to as the "copper scheme"). First, the shift in lasing wavelength due to a change in temperature was investigated. The inset of Fig. 2 shows how the output power of the OP-SDL changed as the temperature of the heat sink was adjusted for a set of tuning wavelengths. Parabolic curves were fitted to the data points and the heat sink temperature for the maximum output power was extracted for each tuning wavelength. These temperatures are shown in Fig. 2 together with a linear fit of the data points. From the linear fit, the shift in wavelength due to a change in temperature, $\mathrm{d}\lambda/\mathrm{d}T$, was calculated to be 0.47 nm/K, which is in accordance with other reports [13], [14]. This is also the wavelength-temperature dependence of the free-running OP-SDL, i.e. one in which no intra-cavity element (birefringent filter) is used to control the wavelength.

Second, the peak wavelength of the emission spectrum of two free-running OP-SDLs, one using the diamond scheme and one using the copper scheme, was recorded for various pump powers. These are shown in Fig. 3, where the horizontal axis shows P_{diss}, the heat power that has to be dissipated from the GE to the heat sink. Assuming steady-state conditions and negligible heat transfer to the surrounding air, P_{diss} is the incident pump power minus the reflected pump power and the output power of the OP-SDL, see the inset in Fig. 3:

$$P_{diss} = P_{pump} - P_{reflected} - P_{out} \tag{1}$$

From the slopes of the linear fits to the data points, the wavelength shift due to a change in dissipated power, $\mathrm{d}\lambda/\mathrm{d}P_{diss}$, was calculated to 1.14 nm/W for the copper scheme and 0.65 nm/W for the diamond scheme. In these measurements the pump spot diameter was 300 μm and 480 μm, the fundamental mode size 210 μm and 420 μm, and the out-coupling reflectance of the external-cavity mirror 99% and 98% for the copper and diamond schemes, respectively.

From these investigations, we can estimate the thermal impedance of the heat removal schemes:

$$Z_{th} = \frac{\mathrm{d}T}{\mathrm{d}P_{diss}} = \frac{\mathrm{d}\lambda/\mathrm{d}P_{diss}}{\mathrm{d}\lambda/\mathrm{d}T} \tag{2}$$

For the heat sink with the copper heat spreader the thermal impedance was calculated to be Z_{th}^{copper} =2.4 K/W and with the diamond heat spreader $Z_{th}^{diamond}$ =1.4 K/W, which is in accordance with previous results [15] and shows that using a diamond heat spreader is a significant improvement and should be beneficial for the performance of the OP-SDL.

To validate that these numbers were realistic, the temperature distribution was also numerically calculated in a finite element model (FEM). For simplicity, the geometry of the heat removal structures was approximated to be cylindrically symmetric; the assumed structures for the copper and diamond schemes are shown in Figs. 4 and 5, respectively. The lowest boundary of each structure was held at a constant temperature while all other boundaries were insulating. The heat from the optical pumping was modeled as a Gaussian-shaped heat source in the topmost layer,

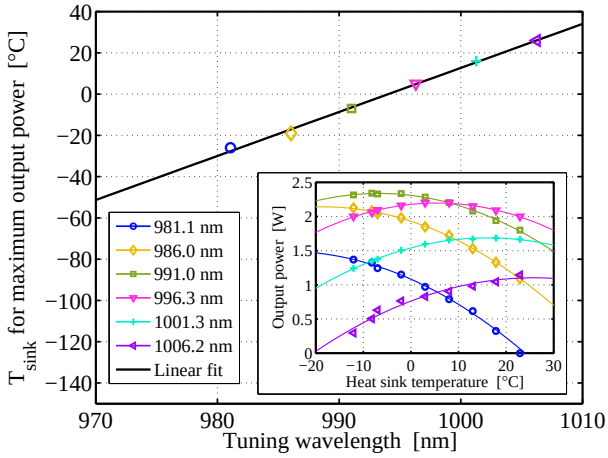

Fig. 2. Determination of the wavelength shift as a function of heat sink temperature. The inset shows data points and parabolical fits thereof from measurements of output power vs. heat sink temperatures at different wavelengths. The heat sink temperature that corresponds to the maximum output power for each wavelength is plotted in the main figure together with a linear fit; from the slope the wavelength variation with temperature is calculated to be $d\lambda/dT$ =0.47 nm/K.

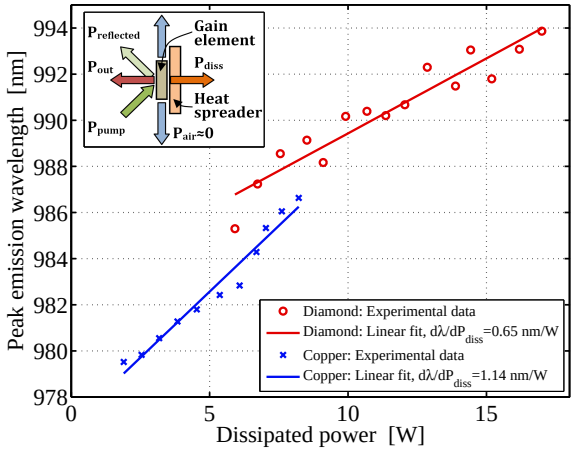

Fig. 3. Peak wavelength of the emission from free-running OP-SDLs with the GEs mounted on copper and diamond heat spreaders as a function of dissipated power. The inset illustrates the mechanisms of the power flux into and out of the GE.

the 7 μm thick GE, with a $1/e^2$-radius, R_{source}, equal to half the diameter of the pump spot in the measurements with the diamond scheme, i.e. R_{source} =240 μm. For the thermal conductivities of copper and CVD diamond 400 W/(K·m) and 2000 W/(K·m) were used, respectively. Figures 6 and 7 show the temperature distribution in the heat spreading regions at P_{diss} =10 W.

By changing the pump power in the simulations, the corresponding change of the temperature in the active region could be calculated; the ratio of this temperature change and the change in pump power giving the thermal impedance. The so obtained values were $Z_{th,FEM}^{copper}$ =3.5 K/W and $Z_{th,FEM}^{diamond}$ =1.2 K/W, respectively, for the copper and diamond schemes, in good agreement with the measurements considering the approximations and the uncertainty in the detailed shape of the pump beam intensity cross section. Obviously, the diamond slab is an efficient transporter of the heat in the lateral direction, which explains the considerably better heat transport capacity of

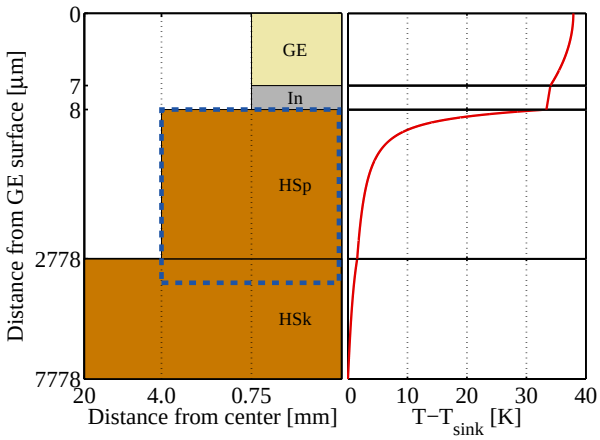

Fig. 4. Cross-section of the modeled heat sink with the copper heat spreader and the temperature profile of the vertical symmetry axis. The maximum temperature difference between the active region and the heat sink is 38 K. GE: Gain element, In: Indium solder, HSp: Copper heat spreader, HSk: Copper heat sink. Note that some of the axes are not to scale. Isotherms for the area in the dashed rectangle are shown in Fig. 6.

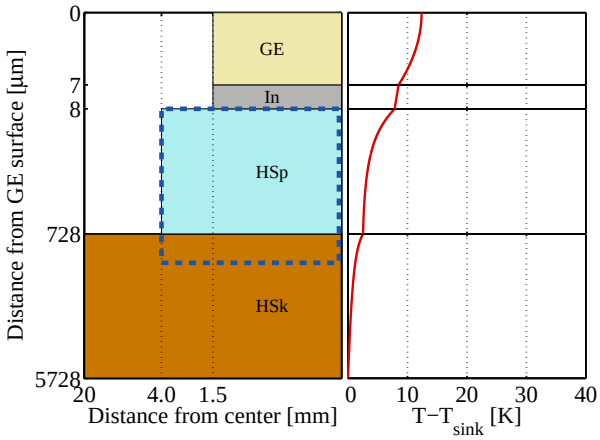

Fig. 5. Cross-section of the modeled heat sink with the diamond heat spreader and the temperature profile of the vertical symmetry axis. The maximum temperature difference between the active region and the heat sink is 12 K. GE: Gain element, In: Indium solder, HSp: Diamond heat spreader, HSk: Copper heat sink. Note that some of the axes are not to scale. Isotherms for the area in the dashed rectangle are shown in Fig. 7.

the diamond heat sink.

4. OP-SDL Performance

The basic performance of the free-running OP-SDL with a diamond-mounted broadband GE was evaluated in a linear cavity configuration with a plano-convex external mirror with 300 mm radius of curvature and 98% reflectance. The cavity length was about 105 mm, causing the waist diameter of the cavity field (the fundamental transverse mode) on the GE to be $\sim$420 μm. The GE was pumped by light from an 808 nm wavelength laser focused to a spot of approximately 480 μm diameter. Fig. 8 shows the power characteristics for the free-running OP-SDL. The threshold

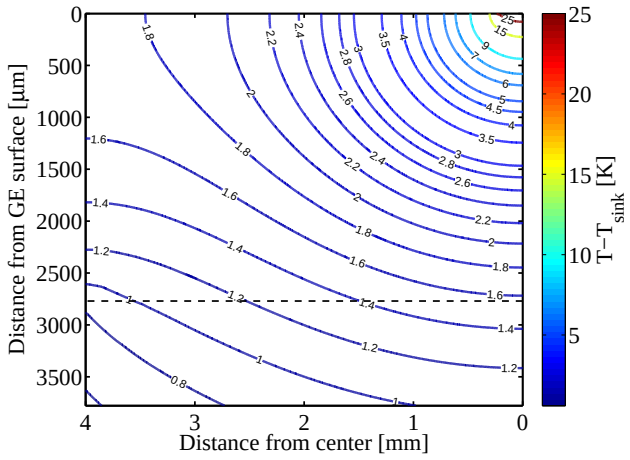

Fig. 6. Isotherms for $T - T_{sink}$ in a cross-section of the heat sink with the copper heat spreader at P_{diss} =10 W. Above the dashed horizontal line is the copper heat spreader and below is the top 1 mm of the copper heat sink; this region is marked in Fig. 4 with a dashed rectangle.

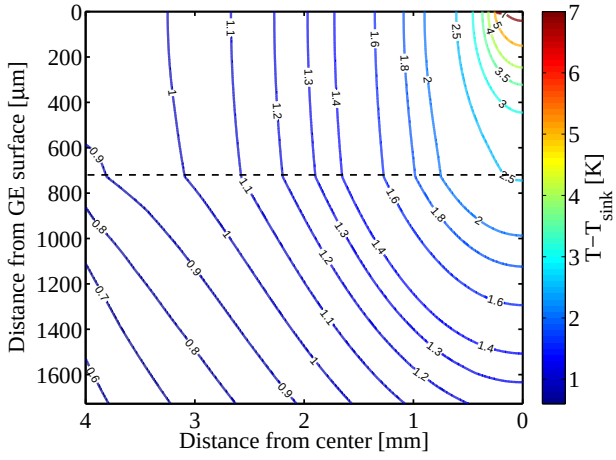

Fig. 7. Isotherms for $T - T_{sink}$ in a cross-section of the heat sink with the diamond heat spreader at P_{diss} =10 W. Above the dashed horizontal line is the diamond heat spreader and below is the top 1 mm of the copper heat sink; this region is also marked in Fig. 5 with a dashed rectangle. The steep angles of the isotherms demonstrate the efficient heat transport in the lateral direction.

pump power (with respect to absorbed pump power) is 5 W, the slope efficiency is 38%, and the maximum output power is 12 W at the highest available absorbed pump power of 37 W. The M^2-value, the beam propagation factor describing the beam quality, is 1.35 and 1.50 at low (7 W) and high (35 W) pump power, respectively. The full width at half maximum (FWHM) of the optical spectra of the free-running OP-SDL were ∼3 nm.

When a 2 mm thick birefringent filter (BRF) was inserted in the cavity, with the surface normal aligned at the Brewster angle to the optical axis, see Fig. 9 for a schematic, it was possible to tune the lasing wavelength of the OP-SDL by rotating the BRF around its surface normal. As can be seen in Fig. 10, the full tuning range is 32 nm, centered at 995 nm, at an absorbed pump power of 35 W, and the peak output power is 7.5 W. With the BRF inserted into the cavity, the spectra narrowed to about 0.6 nm FWHM. The beam quality remained good when inserting the BRF into the cavity, with M^2-values similar to the ones for the free-running laser. These results,

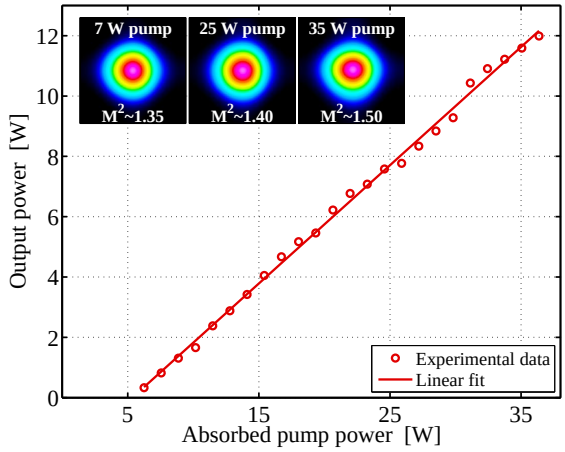

Fig. 8. Power characteristics of a free-running OP-SDL employing a diamond-mounted broadband GE. The insets show beam profiles of the OP-SDL at low (7 W), medium (25 W), and high (35 W) absorbed pump powers; the M^2-values were estimated using a commercial BeamScope instrument to be 1.35, 1.40, and 1.50, respectively. The temperature of the heat sink was set to 15 °C.

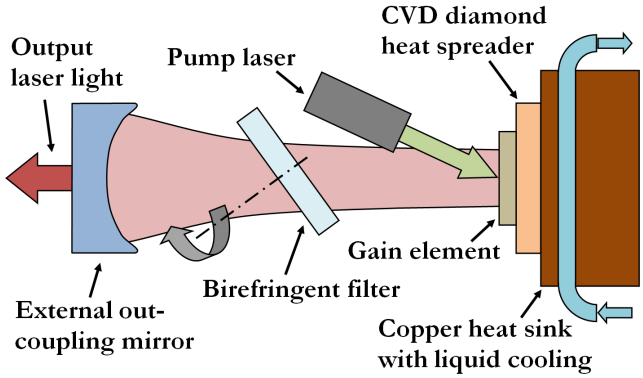

Fig. 9. Schematic view (not to scale) of the setup for the tuning experiments. For the power characteristics experiment, shown in Fig. 8, the birefringent filter was not inserted in the cavity.

employing a diamond heat spreader, represent a great improvement in performance as compared to when a copper heat spreader is employed [10].

5. Conclusion

We have demonstrated wide wavelength tuning at high output power of an OP-SDL with a broadband gain element (GE). As previously described, the GE was designed and optimized for uniform active mirror reflectance over a large range of wavelengths at moderate pump power and low output power from the OP-SDL (at threshold). The experiments show that broadband tuning is also possible at high pump power and high output power, provided that heat is efficiently removed from the GE. To achieve this, the broadband GE was mounted on a CVD diamond heat spreader with indium solder using the flip-chip method. The thermal impedance was reduced from 2.4 K/W to 1.4 K/W as compared to a copper heat spreader. In high-power tuning experiments, the full tuning range was 32 nm (the 3dB tuning range was 25 nm) with good beam quality and a maximum output power at the center of the tuning range (at 995 nm) of 7.5 W.

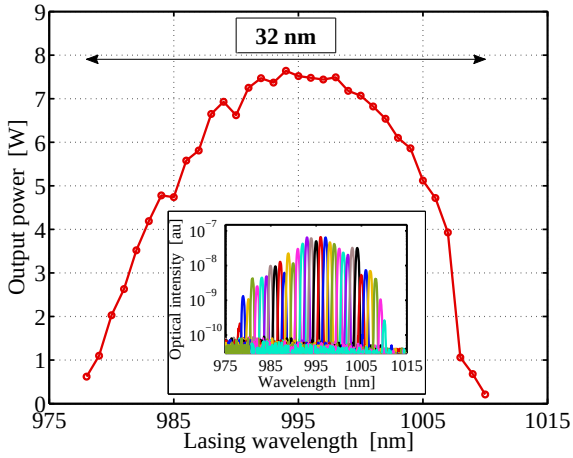

Fig. 10. Results from the high-power tuning experiments with an OP-SDL employing a diamond-mounted broadband GE at an absorbed pump power of 35 W in a 480 μm diameter pump spot. The full tuning range is 32 nm with a peak output power of 7.5 W, and the 3dB tuning range is 25 nm. The temperature of the heat sink was set to 15 °C. The inset shows sample spectra recorded during the tuning experiments.

References

[1] C. E. Wieman and L. Hollberg, "Using diode lasers for atomic physics," *Review of Scientific Instruments*, vol. 62, no. 1, pp. 1–20, Jan. 1991. [Online]. Available: http://dx.doi.org/10.1063/1.1142305

[2] S. Chénais, F. Druon, F. Balembois, P. Georges, R. Gaumé, P. H. Haumesser, B. Viana, G. P. Aka, and D. Vivien, "Spectroscopy and efficient laser action from diode pumping of a new broadly tunable crystal: Yb^{3+}:Sr_3 $Y(BO_3)_3$," *Journal of the Optical Society of America B: Optical Physics*, vol. 19, no. 5, pp. 1083–1091, May 2002. [Online]. Available: http://dx.doi.org/10.1364/JOSAB.19.001083

[3] F. Bertinetto, M.-L. Pascu, M. A. Greco, and M. Bisi, "Studies on tunable lasers as sources for spectroscopy measurements," in *Proc. SPIE*, vol. 2461, no. 1. Bucharest, Romania: SPIE, Mar. 1995, pp. 317–324. [Online]. Available: http://dx.doi.org/10.1117/12.203564

[4] J. D. Berger and D. Anthon, "Tunable MEMS devices for optical networks," *Optics and Photonics News*, vol. 14, no. 3, pp. 42–49, Mar. 2003.

[5] J. Sandusky and S. Brueck, "A CW external-cavity surface-emitting laser," *IEEE Photonics Technology Letters*, vol. 8, no. 3, pp. 313–315, Mar. 1996. [Online]. Available: http://dx.doi.org/10.1109/68.481101

[6] B. Rudin, A. Rutz, M. Hoffmann, D. J. H. C. Maas, A.-R. Bellancourt, E. Gini, T. Südmeyer, and U. Keller, "Highly efficient optically pumped vertical-emitting semiconductor laser with more than 20 W average output power in a fundamental transverse mode," *Optics Letters*, vol. 33, no. 22, pp. 2719–2721, Nov. 2008. [Online]. Available: http://dx.doi.org/10.1364/OL.33.002719

[7] T.-L. Wang, Y. Kaneda, J. M. Yarborough, J. Hader, J. V. Moloney, A. Chernikov, S. Chatterjee, S. W. Koch, B. Kunert, and W. Stolz, "High-power optically pumped semiconductor laser at 1040 nm," *IEEE Photonics Technology Letters*, vol. 22, no. 9, pp. 661–663, May 2010. [Online]. Available: http://dx.doi.org/10.1109/LPT.2010.2043731

[8] L. Fan, M. Fallahi, A. Zakharian, J. Hader, J. Moloney, R. Bedford, J. Murray, W. Stolz, and S. Koch, "Extended tunability in a two-chip VECSEL," *IEEE Photonics Technology Letters*, vol. 19, no. 8, pp. 544–546, Apr. 2007. [Online]. Available: http://dx.doi.org/10.1109/LPT.2007.893898

[9] J. Paajaste, S. Suomalainen, R. Koskinen, A. Härkönen, M. Guina, and M. Pessa, "High-power and broadly tunable GaSb-based optically pumped VECSELs emitting near 2 μm," *Journal of Crystal Growth*, vol. 311, no. 7, pp. 1917–1919, Mar. 2009. [Online]. Available: http://dx.doi.org/10.1016/j.jcrysgro.2008.10.071

[10] C. Borgentun, J. Bengtsson, A. Larsson, F. Demaria, A. Hein, and P. Unger, "Optimization of a broadband gain element for a widely tunable high-power semiconductor disk laser," *IEEE Photonics Technology Letters*, vol. 22, no. 13, pp. 978–980, Jul. 2010. [Online]. Available: http://dx.doi.org/10.1109/LPT.2010.2048309

[11] C. Borgentun, J. Bengtsson, and A. Larsson, "Direct measurement of the spectral reflectance of OP-SDL gain elements under optical pumping," *Optics Express*, vol. 19, no. 18, pp. 16 890–16 897, Aug. 2011. [Online]. Available: http://dx.doi.org/10.1364/OE.19.016890

[12] R. Häring, R. Paschotta, A. Aschwanden, E. Gini, F. Morier-Genoud, and U. Keller, "High-power passively mode-locked semiconductor lasers," *IEEE Journal of Quantum Electronics*, vol. 38, no. 9, pp. 1268–1275, Sep. 2002. [Online]. Available: http://dx.doi.org/10.1109/JQE.2002.802111

[13] A. Garnache, A. A. Kachanov, F. Stoeckel, and R. Houdré, "Diode-pumped broadband vertical-external-cavity surface-emitting semiconductor laser applied to high-sensitivity intracavity absorption spectroscopy," *Journal of the*

Optical Society of America B: Optical Physics, vol. 17, no. 9, pp. 1589–1598, Sep. 2000. [Online]. Available: http://dx.doi.org/10.1364/JOSAB.17.001589

[14] O. G. Okhotnikov, "Tailoring the wavelength of semiconductor disk lasers," in *Proc. SPIE*, vol. 7919, no. 1. San Francisco, California, USA: SPIE, Feb. 2011, pp. 79 190U–17. [Online]. Available: http://dx.doi.org/10.1117/12.873167

[15] A. Chernikov, J. Herrmann, M. Koch, B. Kunert, W. Stolz, S. Chatterjee, S. W. Koch, T.-L. Wang, Y. Kaneda, J. M. Yarborough, J. Hader, and J. V. Moloney, "Heat management in high-power vertical-external-cavity surface-emitting lasers," *IEEE Journal of Selected Topics in Quantum Electronics*, vol. PP, no. 99, pp. 1–7, 2011. [Online]. Available: http://dx.doi.org/10.1109/JSTQE.2011.2115995